

Mechanochemical Topological Defects in an Active Nematic

Michael M. Norton^{1,*} and Piyush Grover²

¹*School of Physics and Astronomy, Rochester Institute of Technology, Rochester, New York 14623, USA*

²*Mechanical and Materials Engineering, University of Nebraska–Lincoln, Lincoln, Nebraska 68588, USA*

(Dated: Friday 23rd December, 2022)

We propose a reaction-diffusion system that converts topological information of an active nematic into chemical signals. We show that a curvature-dependent reaction dipole is sufficient for creating a system that dynamically senses topology by producing a scalar order parameter possessing local extrema coinciding with $\pm\frac{1}{2}$ defects. We consider two possible physical origins of such dipoles: (i) curved molecules that preferentially bind to nematic regions matching their curvature and (ii) nematic molecules that become reaction dipoles when deformed. We demonstrate the behavior of this system for stationary defects and in the presence of hydrodynamic flows as seen in active nematics. The model can help generate testable hypotheses for biological phenomena and motivate the creation of bioinspired materials that dynamically couple nematic structure with biochemistry.

Biological matter is defined by tightly integrated chemical and chemomechanical feedback loops that give rise to robust self-organized dynamics. These dynamical pathways transform genotype into phenotype, enabling reproduction of highly specific body plans, wound healing, and the ability of organisms to respond effectively to environmental stimuli. The field of active matter seeks to gain an understanding of the principles underpinning these phenomena to advance biology and develop design principals for self-organizing materials. An important class of active materials are active nematics. Composed of anisotropic constituents, active nematics are characterized by their complex hydrodynamic flows and accompanying topological defect dynamics. In extensile active nematics, defects are created spontaneously through the Simha-Ramaswamy bend instability [1]. The different symmetries of the $+\frac{1}{2}$ (polar) and $-\frac{1}{2}$ (trifold) defects change the nature of the forces and flow fields generated by each, leading to rich dynamics in both biological and reconstituted systems [2–5].

In biology, defects can take on additional significance. In bacterial biofilms, the high stresses that accompany topological defects generate three-dimensional, multicellular fruiting bodies [6, 7]. In eukaryotic organisms, these stresses correlate with increased apoptosis in epithelial cells [8], and in neural tissue, flocking neural progenitor cells tend to accumulate near $+\frac{1}{2}$ defects while avoiding $-\frac{1}{2}$ defects [9]. Despite the complexity and variety of these living systems, the velocity fields and buckling phenomena are well captured by relatively simple solid [6] or fluid-based continuum models [7, 8].

In contrast to the disordered defect-laden flows in biofilms, defect arrangements in the hydra’s supracellular acto-myosin network are highly structured and locate its limbs, mouth, and foot. The organism cited by Turing as an exemplar of biological pattern formation has remained a model for morphogenesis because the locations of these defects are robust to destructive perturbations,

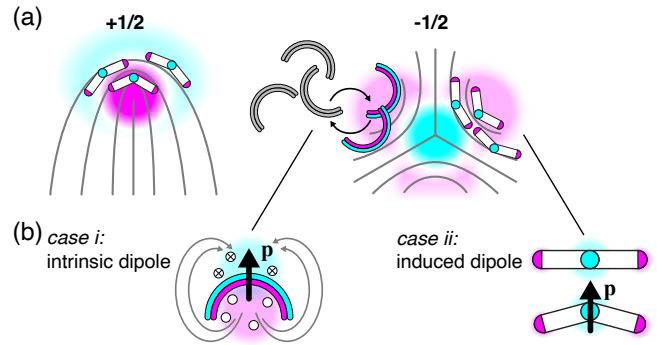


FIG. 1. (a) schematic showing desired behavior of the defect sensing system: concentration extrema located at defect cores; (b) two possible physical manifestations of chemical dipoles: (i) an intrinsically curved enzyme with both a physical and chemical polarity \mathbf{p} that only binds to the nematic at regions of preferred geometry and (ii) a nematic enzyme that acquires a chemical dipole when deformed. In both (i) and (ii), the magenta side produces a product while the cyan side consumes it.

permitting repeatable experiments [10–13]. In the language of dynamical systems, hydra are able to regenerate their form from many initial conditions, suggesting that their body plan is a form of dynamical attractor. Since robustness can only be achieved through feedback mechanisms, researchers have suggested that defects are effectively *mechanical morphogens* that transduce large scale structural information back down to the biochemical scale [11, 12]. Recently, Vafa and Mahadevan proposed that two-way coupling between defects and the curvature of an active shell is sufficient to stabilize hydra-like limb patterns [14]. How these new insights connect to previous observations of biochemical patterning in the hydra remain unclear [15]. More generally, a number of recent models and experiments have explored how various combinations of curvature, topology, mass transport, and biochemical dynamics enable pattern formation and shape sensing [16–27].

Motivated by observations of hydra morphogenesis and

* mike.m.norton@gmail.com

numerous possible modes of coupling between form and chemical activity, we ask the question: can a simple mechanochemical feedback scheme *identify* topological defects in a planar, uniaxial active nematic? Defects can readily be identified by eye or by algorithmically calculating the winding number of a region [28, 29], but both suppose a whole picture view of the material. We propose a bioinspired solution that utilizes reaction-diffusion processes that depend on local geometric features of the embedding nematic. The output of this system is a scalar concentration field with local extrema coinciding with the cores of $\pm\frac{1}{2}$ defects. Fig. 1a shows the idealized behavior, similar to the topological charge density proposed in [30], for which we will develop a dynamical model.

At the heart of the system are reaction dipoles (infinitesimal source-sink pairs) that are oriented by the nematic director in such a way as to break source-sink symmetry at defects. The net effect of the distribution of these dipoles is the spontaneous highlighting of regions containing $\pm\frac{1}{2}$ defects. We consider two physical manifestations governed by only slightly different models. In *case i*, the dipoles are intrinsically curved molecules that bind to the nematic in a curvature-dependent manner, Fig. 1b. Alternatively, in *case ii* we consider nematic constituents that gain chemical polarity when deformed. Importantly, the reactions in both cases continuously churn through reactants. Thus, the defect sensing system we propose is itself a non-equilibrium system. With topological information converted into a concentration field, one can envision many possibilities for topology-dependent dynamics that take this field as an input. This work therefore serves as a scaffold upon which more complex chemomechanical loops can be proposed and motivates experiments in both ground-up and biological systems.

Nematohydrodynamic Model. The evolution of the nematic director field is governed by active nematohydrodynamic equations in the high Ericksen and low Reynolds number limits [31, 32]. The nematic order is represented by the traceless and symmetric second order tensor $\mathbf{Q} = s[\mathbf{n} \otimes \mathbf{n} - \mathbf{I}/2]$ where \mathbf{n} is the nematic orientation and $s = \sqrt{2\mathbf{Q} : \mathbf{Q}}$ is the degree of order. Momentum conservation and incompressibility govern the fluid flow \mathbf{u} and hydrostatic pressure p

$$\begin{aligned} \partial_t \mathbf{Q} + \mathbf{u} \cdot \nabla \mathbf{Q} + [\boldsymbol{\Omega}, \mathbf{Q}] - \lambda \mathbf{E} &= (1 - s^2) \mathbf{Q} + \nabla^2 \mathbf{Q}, \\ \nabla^2 \mathbf{u} - \nabla p - \alpha \nabla \cdot \mathbf{Q} - \xi \mathbf{u} &= 0, \nabla \cdot \mathbf{u} = 0, \end{aligned} \quad (1)$$

where $2\Omega_{ij} = \partial_i u_j - \partial_j u_i$ and $2E_{ij} = \partial_i u_j + \partial_j u_i$ are, respectively, the anti-symmetric and symmetric parts of the flow field gradient, ξ is the strength of substrate friction, $[\dots]$ is the commutator, and $\lambda = 1$ is the flow alignment parameter.

Defect Sensing System. The defect detection chemistry will consist of a few components governed by three PDEs. Throughout, we write as if the species involved are molecular or colloidal in scale. However, we note that system of equations may also be interpreted as the coarse-grained behavior of a biological system. We first examine *case i* and then simplify for *case ii*. All equations

are presented in dimensionless form, where the nematic coherence length and nematic relaxation time have been used, respectively, as the length and time scales [32].

Case i. The first component is a molecule that binds to the nematic in a curvature-dependent manner. We assume that these molecules exist in excess and are free to bind/unbind at rates $k_{\phi\pm}$, where the former depends on the geometry of \mathbf{Q} . Dynamics are given by the transport equations

$$\partial_t \phi + \mathbf{u} \cdot \nabla \phi = D_\phi \nabla^2 \phi + k_{\phi+}(\kappa) - k_{\phi-} \phi, \quad (2)$$

$$k_{\phi+}(\kappa) = k_0 (1 - \phi) e^{-(\kappa - \kappa_0)^2 / \delta}, \quad (3)$$

$$\kappa = Q_{ij} Q_{ik,j} Q_{kl,l}. \quad (4)$$

We assume that the molecules possess intrinsic curvature and will bind to regions of \mathbf{Q} that match their geometry. For perfectly ordered nematics, the quantity $|\mathbf{n} \times (\nabla \times \mathbf{n})|$ measures local bend [33]. In our case, we need a measure in terms of \mathbf{Q} that does not diverge near defects. We choose the scalar invariant κ (Eqn. 4) because it is the lowest order term that breaks splay-bend degeneracy [34, 35]. Typically, this term combines with others to represent the total bending energy; we use it in isolation here as a minimal geometric selection criteria. We manually tune κ_0 to select regions of high bend distortion outside defect cores, Fig. S1. We define specificity of binding using the nonlinear function Eqn. 3, where δ defines the degree of specificity. The factor $(1 - \phi)$ sets the carrying capacity.

We require that these molecules bind to the director with a preferred orientation. We enforce this property by introducing the polar order parameter \mathbf{p} , which encodes both orientation and degree of polar order. We use a lyotropic bulk free energy term that builds polar order where ϕ surpasses a critical concentration ϕ_c and penalizes distortions

$$\begin{aligned} \mathcal{F}_p &= E_{p1} \frac{1}{4} \left(|\mathbf{p}|^2 + 1 - \frac{\phi}{\phi_c} \right) |\mathbf{p}|^2 + E_{p2} \frac{1}{2} |\nabla \mathbf{p}| \\ &+ E_{pQ1} \frac{1}{2} (\mathbf{p} \otimes \mathbf{p}) : \mathbf{Q} + E_{pQ2} (\nabla \cdot \mathbf{Q}) \cdot \mathbf{p}. \end{aligned} \quad (5)$$

In analogy with polarization that arises in flexoelectric and bent-core nematics, we introduce $\mathbf{p} - \mathbf{Q}$ coupling terms [36–39]. We align the molecules perpendicular to the director field through the term $E_{pQ1} > 0$. The following term, $\propto \nabla \cdot \mathbf{Q}$, breaks $\mathbf{p} \perp \mathbf{n}$ degeneracy; we arbitrarily choose $E_{pQ2} > 0$ so that \mathbf{p} will point towards (away from) $- (+)\frac{1}{2}$ defects; see Fig. S1 for details. For simplicity, we assume that the bound molecules apply negligible torque to the nematic such that the dynamics of \mathbf{Q} and \mathbf{u} are independent of ϕ and \mathbf{p} . The dynamics of \mathbf{p} are then given by combination of gradient descent and convective dynamics

$$\begin{aligned} \partial_t \mathbf{p} + \mathbf{u} \cdot \nabla \mathbf{p} + \boldsymbol{\Omega} \mathbf{p} &= -\frac{1}{\gamma} \frac{\delta \mathcal{F}_p}{\delta \mathbf{p}} = \beta_{p1} \left(\frac{\phi}{\phi_c} - 1 - |\mathbf{p}|^2 \right) \mathbf{p} \\ &+ \beta_{p2} \nabla^2 \mathbf{p} - \beta_{pQ1} \mathbf{Q} \mathbf{p} - \beta_{pQ2} \nabla \cdot \mathbf{Q}, \end{aligned} \quad (6)$$

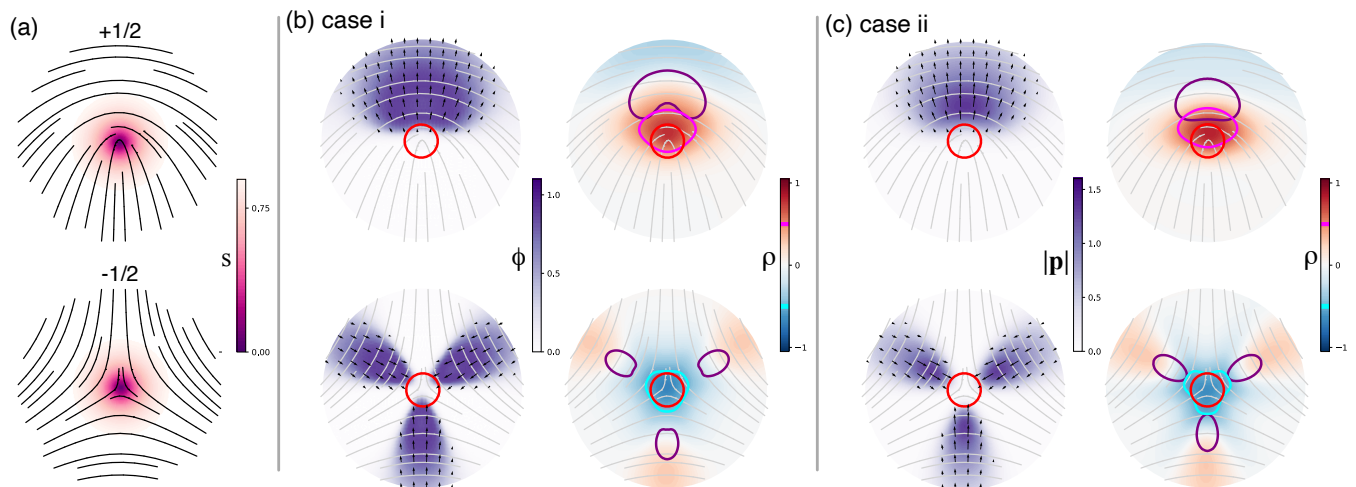


FIG. 2. Idealized behavior for isolated for $\pm\frac{1}{2}$ (top/bottom row) topological defects: panel (a) shows the director \mathbf{Q} and order s ; (b) left column shows the concentration of bound enzymes ϕ and their orientation \mathbf{p} (for $|\mathbf{p}| > 0.3$), right column shows the resulting concentration field ρ and select contours showing $|\mathbf{p}| = 1$ (purple) and $\rho = \pm 0.5$ (magenta, cyan); (c) shows the same as (b) except the color field in the left column shows $|\mathbf{p}|$ instead of ϕ .

where $\beta_{\dots} = \gamma^{-1}E_{\dots}$. The color field in Fig. 2 shows the steady state concentration field of ϕ and the arrows \mathbf{p} around stationary $\pm\frac{1}{2}$ defects.

Finally, we consider the chemical activity of the curved molecules. In addition to geometric polarity, the bound molecules are enzymatically active reaction-dipoles that catalyze the production and destruction of a species a on their interior (head) and exterior (tail) sides, respectively. We will additionally include a background process that maintains a concentration a_0 , so we focus on the dynamics of the deviation $\rho = (a - a_0)/a_0$. Analogous to polarization charge in electrostatics, no net production or depletion of a occurs where the dipole distribution $\phi\mathbf{p}$ is uniform in both strength and orientation. However, where distortions in composition and orientation exist, such as at the boundaries of regions of high ϕ , symmetry is broken and the reaction is biased depending on the local orientation of the molecules. Formally, the polarization charge density-like term $\nabla \cdot (\phi\mathbf{p})$ drives changes in ρ . The full transport equation for ρ is given by

$$\partial_t \rho + \mathbf{u} \cdot \nabla \rho = k_{\rho+} \nabla \cdot (\phi\mathbf{p}) - k_{\rho-} \rho + D_{\rho} \nabla^2 \mu_{\rho}, \quad (7)$$

$$\mu_{\rho} = \gamma_{\rho} \nabla^2 \rho + (s - s_c) \rho + A \rho^2 + \rho^3. \quad (8)$$

where the reaction $k_{\rho-}$ scales a background process that drives $\rho \rightarrow 0$ ($a \rightarrow a_0$) and μ_{ρ} is the chemical potential. We let the Cahn-Hilliard chemical potential depend on the nematic order parameter such that phase separation is only promoted in defect cores where $s < s_c$. Both μ_{ρ} and $k_{\rho-}$ serve to localize ρ to defect cores, enhancing its contrast and efficacy as a sensor. Fig. S2 shows that without an attractive potential, regions of $\pm\rho$ still correlate with defects, but with less pronounced locality and intensity. With the attractive potential, we show in Fig. S3 that ρ is less sensitive to parameter choices for D_{ρ} and $k_{\rho-}$. Finally, we tune the roots of μ_{ρ} with A

to symmetrize the extrema of ρ for $\pm\frac{1}{2}$ defects, Fig. S4. The $-\frac{1}{2}$ defects do not possess clearly defined regions of curvature when hydrodynamics are present, leading to a weaker ρ signal. Overall, we find that the desired behavior of the system is maintained over a range of parameter values.

Case ii. To model the second case in which chemical polarization is induced directly by local bend rather than through an additional species ϕ , only small modifications to the governing equations are needed. First, we omit ϕ dynamics (Eqns. 2-3) and replace the ϕ -dependent term in Eqn. 5 with κ/κ_0 such that the bulk free energy becomes

$$\mathcal{F}_{\mathbf{p},\text{bulk}} = E_{\text{p1}} \left(1 + |\mathbf{p}|^2 - \frac{\kappa}{\kappa_0} \right) |\mathbf{p}|^2, \quad (9)$$

where κ_0 now serves as the critical curvature at which polar order can be created. Lastly, the polarization density term in Eqn. 8 is simplified to $\nabla \cdot \mathbf{p}$.

To demonstrate the behavior of the system, we first consider the steady state behavior of the equations for idealized defects. To create the defects, we prescribe anchoring conditions along a circle inscribed within the square computational domain with height and width 10 that promote the desired charge and solve Eqns. 1-8 with $\alpha = 0$. All simulations are performed using the open source spectral-based solver Dedalus [40]. Fig. 2 shows that cases *i* and *ii* behave similarly. The left column of case *i* shows the concentration of bound molecules ϕ (purple) and their orientation \mathbf{p} (arrows). The $+$ ($-$) $\frac{1}{2}$ defects display one(three) lobes corresponding to regions of preferred curvature. The red circle throughout all panels indicates the defect core size by plotting the $s = 0.5$ level-set. For case *ii*, contours of $|\mathbf{p}|$ are plotted instead of ϕ , but show a similar spatial pattern. The right columns

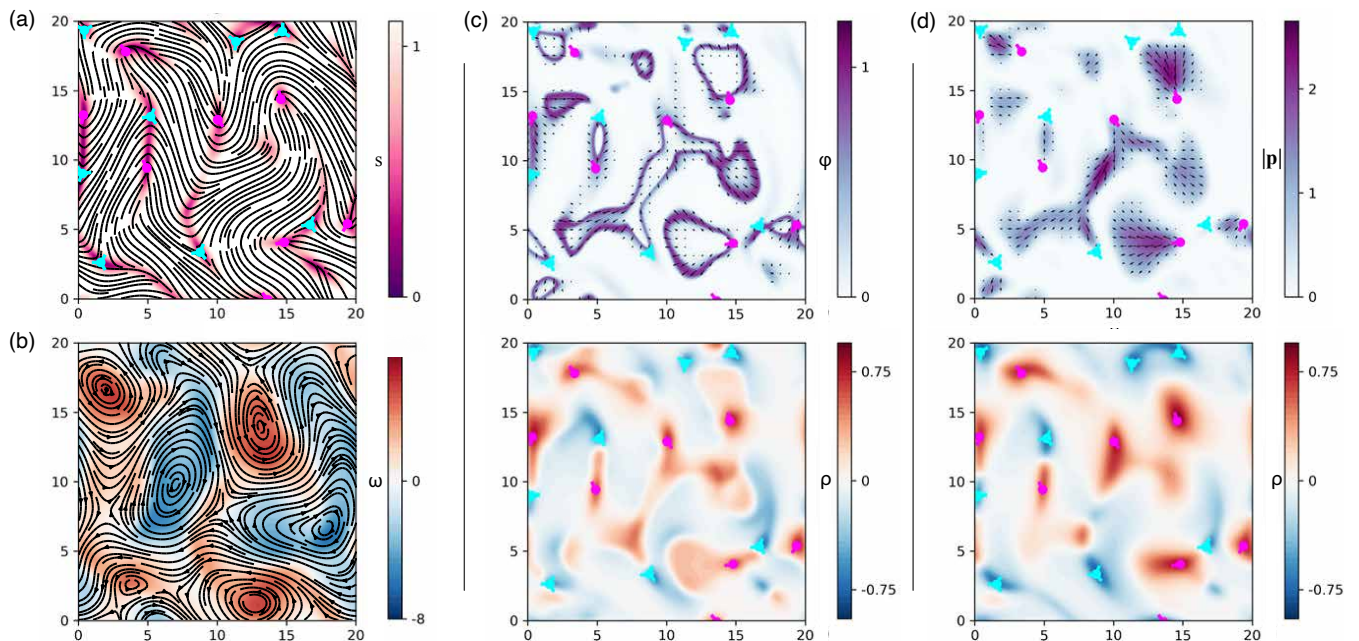


FIG. 3. (a) snapshot of \mathbf{Q} and s with $\pm\frac{1}{2}$ defects labeled with magenta arrows and cyan triangular glyphs; (b) corresponding active flow \mathbf{u} and vorticity ω ; (c) *case i*: ϕ and \mathbf{p} (top) and ρ (bottom), see Movie S1; (d) *case ii*: $|\mathbf{p}|$ and \mathbf{p} (top) and ρ (bottom), see Movie S2.

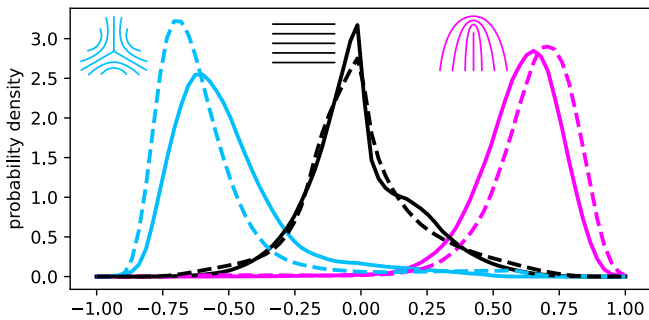


FIG. 4. Probability density function of ρ in regions containing $-\frac{1}{2}$ defects (blue), $+\frac{1}{2}$ defects (magenta), or no defects (black) quantifies the performance of the defect detection system for *case i* (solid) and *case ii* (dashed). Regions are considered belonging to a defect if they fall within one nematic coherence length of a defect core ($l_c = 1$ in our simulations).

of each case show the distribution of ρ . Purple contours highlight the $|\mathbf{p}| = 1$ level-set and approximate boundaries of the dipole-rich regions. Cyan and magenta contours, $\rho^* = \pm 0.5$, emphasize the asymmetry of the resulting concentration field around each defect: $|\rho| > |\rho^*|$ inside defects core and $|\rho| < |\rho^*|$ outside.

We now consider the dynamic scenario (see Movies S1,S2). For simplicity, we choose parameters such that reaction and diffusive dynamics dominate over convective transport, Table S1. The hydrodynamic flows created by activity result in continuous creation and annihilation of $\pm\frac{1}{2}$ defect pairs; Fig. 3a,b show typical nematic order and flow fields. Defects rarely possess geometry identical to their idealized forms considered in Fig. 2. Conse-

quently, the concentration of bound molecules ϕ (*case i*, Fig. 3c-top) and the degree of polar order $|\mathbf{p}|$ (*case ii*, Fig. 3d-top) take on large-scale, complex forms that populate the space between defects. Despite this, the orientation of the reaction dipoles near the defects is sufficient for both systems to report on their topological environments, Fig. 3c,d-bottom. To quantify the performance of the two systems, we plot histograms of ρ within circles of unit radius around each defect and compare that to the distributions of all regions outside those circles. Fig. 4 shows that the positions of defects correlate strongly with the extremal values of the reporting field ρ : the defect-less regions rarely contain $\rho \neq 0$ and the regions containing defects only contain ρ of the appropriate sign. In Figs. S3 and S4 we briefly explore other parameter combinations and show that the qualitative behavior is preserved over a range of conditions.

Discussion and Conclusion. Steering the dynamics of active materials requires strategies distinct from those for near-equilibrium systems. Experimental and computational works have recently demonstrated that spatiotemporally actuating local force generation offers new avenues for both ad hoc [41–43] and computationally-derived control schemes [25, 44, 45]. However, the latter have relied on externally-sensed global flow field or director information to devise their respective, exogenously-implemented control strategies. In order to create truly autonomous biopolymeric materials [34, 46–50], the control must be implemented endogenously, only relying on internal local sensing.

By demonstrating that a material’s topological state can be read internally, we posit that leveraging system’s

biology for the creation of novel materials becomes more accessible. For example, the biochemical basis of many fundamental functional motifs, such as oscillators and switches, is known [51]. One can envision chaining together such elements with ρ to create spatiotemporally complex dynamics that pattern the active stress strength α . The theory of passivity and port-Hamiltonian systems may provide additional tools for rationally designing and analyzing closed-loop PDE systems [52, 53]. It remains to be seen what kinds of control tasks can be accomplished by coupling α to ρ (either directly or through intermediary processes). For instance, can one stabilize an unstable flow state or create pathways that connect existing states [4, 44]?

We close by briefly addressing potential biological implications. While it remains unknown to what degree living systems sense defects, the simplicity of coupling between coarse-grained fields (curvature, polarity, and nematic order) is compelling and may help generate testable hypotheses. Further, we note that intermediate dynamics of ϕ and \mathbf{p} are just as rich as the defect sensor ρ . We suggest that the epiphenomenal structures

created by these fields (top row of Fig. 3c,d) behave as simple organelles because they are constructed on-demand, perform a clear function, and then disassemble as conditions evolve. Taken together, our proposed coupling between structural and chemical anisotropy in active nematics create rich dynamics that can inspire biological explorations and the development of functional mechanochemical materials.

ACKNOWLEDGMENTS

We thank the participants and organizers (Linda Hirst and Kevin Mitchell) of the Telluride 2021 Workshop *Non-linear Dynamics of Active Matter*, and the Brandeis University MRSEC 2022 Winter School for discussions that inspired this work. This material is based upon work supported by the U.S. Department of Energy, Office of Science, Office of Basic Energy Sciences under Award No. DE-SC0022280.

-
- [1] R. Aditi Simha and S. Ramaswamy, “Hydrodynamic Fluctuations and Instabilities in Ordered Suspensions of Self-Propelled Particles,” *Physical Review Letters*, vol. 89, p. 058101, jul 2002.
- [2] M. C. Marchetti, J. F. Joanny, S. Ramaswamy, T. B. Liverpool, J. Prost, M. Rao, and R. A. Simha, “Hydrodynamics of soft active matter,” *Reviews of Modern Physics*, vol. 85, no. 3, pp. 1143–1189, 2013.
- [3] S. J. DeCamp, G. S. Redner, A. Baskaran, M. F. Hagan, and Z. Dogic, “Orientational order of motile defects in active nematics,” *Nature Materials*, vol. 14, pp. 1110–1115, aug 2015.
- [4] C. G. Wagner, M. M. Norton, J. S. Park, and P. Grover, “Exact Coherent Structures and Phase Space Geometry of Preturbulent 2D Active Nematic Channel Flow,” *Physical Review Letters*, vol. 128, p. 028003, jan 2022.
- [5] R. Alert, J. Casademunt, and J. F. Joanny, “Active Turbulence,” *Annual Review of Condensed Matter Physics*, vol. 13, pp. 143–170, 2022.
- [6] Y. I. Yaman, E. Demir, R. Vetter, and A. Kocabas, “Emergence of active nematics in chaining bacterial biofilms,” *Nature Communications*, vol. 10, no. 1, pp. 1–9, 2019.
- [7] K. Copenhagen, R. Alert, N. S. Wingreen, and J. W. Shaevitz, “Topological defects promote layer formation in *Myxococcus xanthus* colonies,” *Nature Physics*, vol. 17, no. 2, pp. 211–215, 2021.
- [8] T. B. Saw, A. Doostmohammadi, V. Nier, L. Kocgozlu, S. Thampi, Y. Toyama, P. Marcq, C. T. Lim, J. M. Yeomans, and B. Ladoux, “Topological defects in epithelia govern cell death and extrusion,” *Nature*, vol. 544, no. 7649, pp. 212–216, 2017.
- [9] K. Kawaguchi, R. Kageyama, and M. Sano, “Topological defects control collective dynamics in neural progenitor cell cultures,” *Nature*, vol. 545, no. 7654, pp. 327–331, 2017.
- [10] A. M. Turing, “The chemical basis of morphogenesis,” *Bulletin of Mathematical Biology*, vol. 52, no. 1-2, pp. 153–197, 1990.
- [11] E. Braun and K. Keren, “Hydra Regeneration: Closing the Loop with Mechanical Processes in Morphogenesis,” *BioEssays*, vol. 40, no. 7, pp. 1–12, 2018.
- [12] Y. Maroudas-Sacks, L. Garion, L. Shani-Zerbib, A. Livshits, E. Braun, and K. Keren, “Topological defects in the nematic order of actin fibres as organization centres of Hydra morphogenesis,” *Nature Physics*, vol. 17, no. February, 2020.
- [13] Y. Maroudas-Sacks and K. Keren, “Mechanical Patterning in Animal Morphogenesis,” *Annual Review of Cell and Developmental Biology*, vol. 37, pp. 469–493, oct 2021.
- [14] F. Vafa and L. Mahadevan, “Active Nematic Defects and Epithelial Morphogenesis,” *Physical Review Letters*, vol. 129, p. 098102, aug 2022.
- [15] H. Meinhardt, “Turing’s theory of morphogenesis of 1952 and the subsequent discovery of the crucial role of local self enhancement and long-range inhibition,” *Interface Focus*, vol. 2, no. 4, pp. 407–416, 2012.
- [16] J. Halatek and E. Frey, “Rethinking pattern formation in reaction-diffusion systems,” *Philosophical Transactions of the Royal Society B: Biological Sciences*, vol. 373, no. 1747, pp. 507–514, 2018.
- [17] F. J. Schwarzendahl, P. Ronceray, K. L. Weirich, and K. Dasbiswas, “Self-organization and shape change by active polarization in nematic droplets,” *Physical Review Research*, vol. 3, p. 043061, oct 2021.
- [18] D. Khoromskaia and G. Salbreux, “Active morphogenesis of patterned epithelial shells,” *arXiv:2111.12820*, pp. 1–31, 2021.
- [19] A. Zakharov and K. Dasbiswas, “Mechanochemical in-

- duction of wrinkling morphogenesis on elastic shells,” *Soft Matter*, vol. 17, no. 18, pp. 4738–4750, 2021.
- [20] A. R. Singh, T. Leadbetter, and B. A. Camley, “Sensing the shape of a cell with reaction diffusion and energy minimization,” *Proceedings of the National Academy of Sciences of the United States of America*, vol. 119, no. 31, 2022.
- [21] T. Burkart, M. C. Wigbers, W. Laeschkir, and E. Frey, “Control of protein-based pattern formation via guiding cues,” *bioRxiv*, pp. 1–24, 2022.
- [22] R. Alert, A. Martínez-Calvo, and S. S. Datta, “Cellular Sensing Governs the Stability of Chemotactic Fronts,” *Physical Review Letters*, vol. 128, no. 14, p. 148101, 2022.
- [23] G. Salbreux, F. Jülicher, J. Prost, and A. Callan-Jones, “Theory of nematic and polar active fluid surfaces,” *arXiv:2201.09251*, pp. 1–43, 2022.
- [24] M. Bonati, L. D. Wittwer, S. Aland, and E. Fischer-Friedrich, “On the role of mechanosensitive binding dynamics in the pattern formation of active surfaces,” *New Journal of Physics*, vol. 24, no. 7, 2022.
- [25] S. Shankar, V. Raju, and L. Mahadevan, “Optimal transport and control of active drops,” *Proceedings of the National Academy of Sciences*, vol. 119, aug 2022.
- [26] L. Barberi and K. Kruse, “Localized states in active fluids,” *arXiv:2209.02581*, 2022.
- [27] P. W. Miller, D. Fortunato, C. Muratov, L. Greengard, and S. Shvartsman, “Forced and spontaneous symmetry breaking in cell polarization,” *Nature Computational Science*, vol. 2, pp. 504–511, aug 2022.
- [28] P. M. Chaikin and T. C. Lubensky, *Principles of Condensed Matter Physics*. Cambridge, UK: Cambridge University Press, 2003.
- [29] G. P. Alexander, B. G.-g. Chen, E. A. Matsumoto, and R. D. Kamien, “Disclination Loops, Hedgehogs, and All That,” pp. 1–19, 2011.
- [30] M. L. Blow, S. P. Thampi, and J. M. Yeomans, “Biphasic, lyotropic, active nematics,” *Physical Review Letters*, vol. 113, no. 24, 2014.
- [31] A. N. Beris and B. J. Edwards, *Thermodynamics of Flowing Systems*, vol. 36. Oxford University, 1994.
- [32] C. M. Koch and M. Wilczek, “Role of Advective Inertia in Active Nematic Turbulence,” *Physical Review Letters*, vol. 127, no. 26, p. 268005, 2021.
- [33] P.-G. de Gennes and J. Prost, *The Physics of Liquid Crystals*. Oxford University Press, 1995.
- [34] R. Zhang, N. Kumar, J. L. Ross, M. L. Gardel, and J. J. De Pablo, “Interplay of structure, elasticity, and dynamics in actin-based nematic materials,” *Proceedings of the National Academy of Sciences of the United States of America*, vol. 115, no. 2, pp. E124–E133, 2017.
- [35] M. Čopič and A. Mertelj, “Q-tensor model of twist-bend and splay nematic phases,” *Physical Review E*, vol. 101, no. 2, 2020.
- [36] L. Longa and G. Pajak, “Modulated nematic structures induced by chirality and steric polarization,” *Physical Review E*, vol. 93, no. 4, 2016.
- [37] G. Pajak, L. Longa, and A. Chrzanowska, “Nematic twist-bend phase in an external field,” *Proceedings of the National Academy of Sciences of the United States of America*, vol. 115, no. 44, pp. E10303–E10312, 2018.
- [38] P. Rudquist, L. Komitov, and S. T. Lagerwall, “Linear electro-optic effect in a cholesteric liquid crystal,” *Physical Review E*, vol. 50, pp. 4735–4743, dec 1994.
- [39] R. B. Meyer, “Piezoelectric Effects in Liquid Crystals,” *Physical Review Letters*, vol. 22, pp. 918–921, may 1969.
- [40] K. J. Burns, G. M. Vasil, J. S. Oishi, D. Lecoanet, and B. P. Brown, “Dedalus: A flexible framework for numerical simulations with spectral methods,” *Physical Review Research*, vol. 2, p. 023068, apr 2020.
- [41] R. Zhang, S. A. Redford, P. V. Ruijgrok, N. Kumar, A. Mozaffari, S. Zemsky, A. R. Dinner, V. Vitelli, Z. Bryant, M. L. Gardel, and J. J. de Pablo, “Spatiotemporal control of liquid crystal structure and dynamics through activity patterning,” *Nature Materials*, vol. 20, pp. 875–882, jun 2021.
- [42] T. D. Ross, H. J. Lee, Z. Qu, R. A. Banks, R. Phillips, and M. Thomson, “Controlling organization and forces in active matter through optically defined boundaries,” *Nature*, vol. 572, pp. 224–229, aug 2019.
- [43] L. M. Lemma, M. Varghese, T. D. Ross, M. Thomson, A. Baskaran, and Z. Dogic, “Spatiotemporal patterning of extensile active stresses in microtubule-based active fluids,” *arXiv:2209.06277*, 2022.
- [44] M. M. Norton, P. Grover, M. F. Hagan, and S. Fraden, “Optimal Control of Active Nematics,” *Physical Review Letters*, vol. 125, p. 178005, oct 2020.
- [45] M. J. Falk, V. Alizadehyazdi, H. Jaeger, and A. Murugan, “Learning to Control Active Matter,” vol. 033291, no. September, 2021.
- [46] L. M. Lemma, M. M. Norton, A. M. Tayar, S. J. DeCamp, S. A. Aghvami, S. Fraden, M. F. Hagan, and Z. Dogic, “Multiscale Microtubule Dynamics in Active Nematics,” *Physical Review Letters*, vol. 127, p. 148001, sep 2021.
- [47] B. Lemma, N. P. Mitchell, R. Subramanian, D. J. Needleman, and Z. Dogic, “Active microphase separation in mixtures of microtubules and tip-accumulating molecular motors,” 2021.
- [48] G. Lee, G. Leech, M. J. Rust, M. Das, R. J. McGorty, J. L. Ross, and R. M. Robertson-Anderson, “Myosin-driven actin-microtubule networks exhibit self-organized contractile dynamics,” *Science Advances*, vol. 7, no. 6, pp. 1–10, 2021.
- [49] C. P. Hsu, A. Sciortino, Y. A. de la Trobe, and A. R. Bausch, “Activity-induced polar patterns of filaments gliding on a sphere,” *Nature Communications*, vol. 13, no. 1, pp. 1–8, 2022.
- [50] J. Berezney, B. L. Goode, S. Fraden, and Z. Dogic, “Extensile to contractile transition in active microtubule-actin composites generates layered asters with programmable lifetimes,” *Proceedings of the National Academy of Sciences*, vol. 119, p. e2115895119, feb 2022.
- [51] J. J. Tyson, K. C. Chen, and B. Novak, “Sniffers, buzzers, toggles and blinkers: Dynamics of regulatory and signaling pathways in the cell,” *Current Opinion in Cell Biology*, vol. 15, no. 2, pp. 221–231, 2003.
- [52] M. R. Jovanovic, M. Arcak, and E. D. Sontag, “A Passivity-Based Approach to Stability of Spatially Distributed Systems With a Cyclic Interconnection Structure,” *IEEE Transactions on Automatic Control*, vol. 53, pp. 75–86, jan 2008.
- [53] M. Ahmadi, G. Valmorbida, and A. Papachristodoulou, “Dissipation inequalities for the analysis of a class of PDEs,” *Automatica*, vol. 66, pp. 163–171, apr 2016.